Proceedings of GT2005
ASME Turbo Expo 2005: Power for Land, Sea and Air
June 6-9, 2005, Reno-Tahoe, Nevada, USA

GT2005-68900

EFFECTS OF MID-PASSAGE GAP, ENDWALL MISALIGNMENT AND ROUGHNESS ON ENDWALL FILM-COOLING

N. D. Cardwell, N. Sundaram, and K. A. Thole
Mechanical Engineering Department
Virginia Polytechnic Institute and State University
Blacksburg, Virginia 24061 USA.

ABSTRACT

To maintain acceptable turbine airfoil temperatures, film-cooling is typically used whereby coolant, extracted from the compressor, is injected through component surfaces. In manufacturing a turbine, the first stage vanes are cast in either single airfoils or double airfoils. As the engine is assembled, these singlets or doublets are placed in a turbine disk in which there are inherent gaps between the airfoils. The turbine is designed to allow outflow of high pressure coolant rather than hot gas ingestion. Moreover, it is quite possible that the singlets or doublets become misaligned during engine operation. It has also become of interest to the turbine community as to the effect of corrosion and deposition of particles on component heat transfer. This study uses a large-scale turbine vane in which the following two effects are investigated: the effect of a mid-passage gap on endwall film-cooling and the effect of roughness on endwall film-cooling. The results indicate that the mid-passage gap was found to have a significant effect on the coolant exiting from the combustor-turbine interface slot. When the gap is misaligned, the results indicate a severe reduction in the film-cooling effectiveness in the case where the pressure side endwall is below the endwall associated with the suction side of the adjacent vane.

INTRODUCTION

Traditional techniques to cool the hot section of a gas turbine engine involve the use of air from the compressor that has bypassed the combustion chamber and is used for impingement cooling, film-cooling, and convective cooling in the turbine airfoils. The coolant is generally high pressure air that has been routed to the turbine section through a secondary flow path. In the manufacturing of a turbine engine, the airfoils and their associated endwalls are typically cast as singlets or doublets that are then placed in the turbine disk. It is inherently difficult to seal interfaces between the singlets and doublets, particularly when considering the expansion and contraction of turbine components during engine operation. Given there is high-pressure coolant that must be routed to the turbine through a secondary flow path to cool the blades and vanes, this high pressure coolant can also leak through any gaps that may exist in the turbine. Moreover, since combustor profiles are not always uniform it would be expected that the thermal contraction and expansion of adjacent vanes would be significantly different. This difference can lead to turbine airfoils that are misaligned. The question then becomes, how should a turbine designer account for a potential misalignment in airfoil components in their calculations of airfoil temperatures?

Airfoil roughness is an important problem in today's operation of gas turbines. With the push to use fuels other than natural gas, such as coal-derived fuels for industrial turbines, erosion and deposition are issues that must be accounted for. Moreover, propulsive gas turbines are being used in harsh environments in which sand or other foreign debris is ingested and deposited on components in the hot section.

The work presented in this paper compares measured adiabatic effectiveness levels of a well-sealed mid-passage gap that is aligned and misaligned to determine the effect on endwall film-cooling and slot cooling. Also compared in this paper is the effect that roughness can have on endwall film-cooling.

NOMENCLATURE

C	true chord of stator vane
C_a	axial chord of stator vane
D	diameter of film-cooling hole
I	momentum flux ratio
L	length of mid-passage gap
$\dot{m}$	mass flowrate
M	mass flux/ blowing ratio
P	vane pitch; hole pitch
P_o or p	total and static pressures

Re_{in}	Reynolds number defined as $Re = CU_\infty / \nu$
s	distance along vane from flow stagnation
S	span of stator vane
T	temperature
x,y,z	local coordinates
u,v,w	local velocity components
U	velocity global

Greek

η	adiabatic effectiveness, $\eta = (T_\infty - T_{aw}) / (T_\infty - T_c)$
ρ	density
ν	kinematic viscosity
θ	non-dimensionalized gap effectiveness, $\theta = (T_\infty - T_G) / (T_\infty - T_c)$

Subscripts

aw	adiabatic wall
c	coolant conditions
G	gap
in	inlet conditions
j	coolant flow through film-cooling holes
s	flow through upstream slot
∞	freestream conditions

RELEVANT PAST STUDIES

There have been turbine endwall studies in the literature that have documented the effects of an upstream slot, discrete film-cooling holes, and combined upstream slot and film-cooling. Only a few studies exist on the effect of a mid-passage gap. There have been no studies documenting what happens in the case of having a misaligned mid-passage gap in an actual airfoil passage. In addition, there have been no studies on the effect of roughness on endwall film-cooling.

Most of the studies evaluating leakage flows have been concerned with an upstream slot that represents the leakage flow that might occur between the combustor and turbine. Some of the earliest work related to a leakage flow was performed by Blair [1] who used a two-dimensional aligned slot upstream of vane geometry. Enhancements in film-cooling effectiveness along the endwall were observed as the flow through the slot was increased. In a similar study of coolant upstream of a vane passage, Burd et al. [2] studied the effects of an upstream aligned, 45° slot. By using coolant flows as high as 6% of the total passage flow, better cooling was observed over the endwall and on both sides of the vanes relative to lower coolant flows. A study by Colban and Thole [3, 4] measured the effects of changing the combustor liner film-cooling and upstream slot flows on the effectiveness levels along the endwall of a first stage turbine vane. Their results showed that the coolant from the slot was not uniform across the exit with coolant accumulating along the endwall near the suction side of the vane. Coolant injection from the upstream combustor liner caused a different total pressure profile entering the vane passage, relative to a turbulent boundary layer, that in turn changed the secondary flow field.

Detailed endwall film-cooling results have been conducted by Friedrichs et al. [5, 6, and 7]. The results of their first study [5], which were all surface measurements or visualization, indicated a strong influence of the secondary flows on the film-cooling and an influence of the film-cooling on the secondary flows. Their data showed that the angle at which the coolant leaves the hole did not dictate the coolant trajectory except near the hole exit. Furthermore the endwall cross-flow was altered so that the cross-flow was turned toward the inviscid streamlines, which was due to the film-cooling injection.

The only studies to have combined an upstream slot with film-cooling holes in the passage of the vane were those of Zhang and Jaiswal [8], Kost and Nicklas [9], Nicklas [10] and Knost and Thole [11, 12]. One of the most interesting results from the Kost and Nicklas [9] and Nicklas [10] studies was that they found for the slot flow alone, which was 1.3% of the passage mass flow, the horseshoe vortex became more intense. This increase in intensity resulted in the slot coolant being moved off of the endwall surface and heat transfer coefficients that were over three times that measured for no slot flow injection. They attributed the strengthening of the horseshoe vortex to the fact that for the no slot injection the boundary layer was already separated with fluid being turned away from the endwall at the injection location. Given that the slot had a normal component of velocity, injection at this location promoted the separation and enhanced the vortex. Their adiabatic effectiveness measurements indicated higher values near the suction side of the vane due to the slot coolant migration. Knost and Thole reported a significant change in the streamlines in the near endwall region resulting from the upstream slot flow. Their results also indicated that the momentum flux ratio was an important parameter in predicting the cooling jet behavior.

Using a flat plate geometry with no turbine airfoils, Yu and Chyu [13] studied the influence of gap leakage downstream of injection cooling holes. They observed that for a moderate level of film-cooling upstream of a coolant slot, the combined presence with the gap promoted better coolant film protection. However, as the film-cooling flow was increased the coolant from the gap appeared to lift the slot flow coolant from the wall resulting in decreased adiabatic effectiveness.

The only known studies of flow from a slot within the mid-passage of adjacent airfoils were performed by Aunapu et al. [14], Ranson and Thole [15], and Yamao et al. [16]. Aunapu et al. used blowing through a passage gap in an attempt to reduce the effects of a passage vortex. They hypothesized endwall blowing in the blade passage could reduce the effects of the passage vortex. Aunapu et al. [14] observed that endwall jets in the center of the blade passage effectively altered the path of the pressure side leg of the vortex. Unfortunately, the increased blowing caused higher turbulence and higher aerodynamic losses. Ranson and Thole used an aligned mid-passage gap between two adjacent blades for their combined experimental and computational studies. Their results indicated that the flow leaving the gap was directed toward the blade pressure side, as a result of the incoming velocity vector, and then traversed

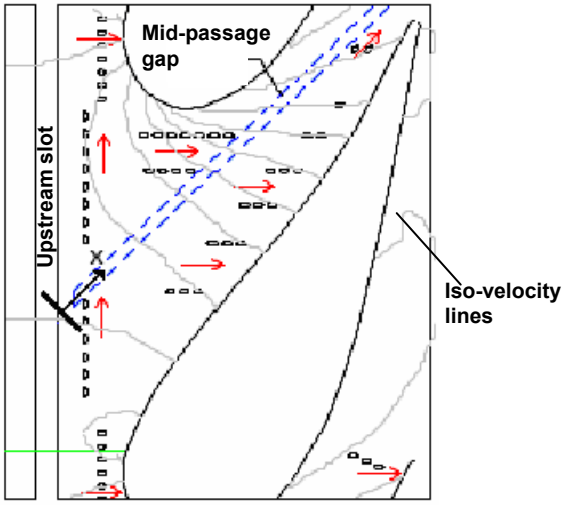

Figure 1. Directions of the coolant hole injection along with iso–velocity contours and the mid-passage gap location for mating two turbine vane platforms.

towards the suction side of the adjacent airfoil. Yamao et al. [16] investigated the distribution of film-cooling effectiveness due to sealing air injected from combustor-vane interface and vane-to-vane interface on annular cascade test equipment. Their study indicated that the film-cooling effectiveness was enhanced with an increase in the sealing air flow rate between the vanes. Also, the increase in sealing air flow rate between the combustor-vane interfaces resulted in significant increase in film-cooling effectiveness near the leading edge but a slight increase along the trailing edge.

In summary, it is important to understand the effect of coolant flow from leakage points in the endwall region under realistic surface conditions to further the technology of turbine blade cooling. To date, there have been only a few studies that have addressed roughness effects on an actual turbine airfoil but none of these studies have addressed the effect of roughness with adiabatic effectiveness levels on a film-cooled endwall.

MID-PASSAGE GAP GEOMETRY

The flat endwall in the linear cascade used for these studies was comprised of five realistic features: a combustor to turbine (upstream) gap, endwall film-cooling, a mid-passage gap with accompanying strip seal, the capability of simulating an endwall misalignment, and surface roughness representative of that found in an engine. The first stage vane endwall film-cooling pattern, which was originally designed and tested by Knost and Thole [12], is shown in Figure 1, which also shows iso-velocity contours and hole injection angles. All film-cooling holes were at an angle of 30° with respect to the endwall surface.

Also included in the endwall pattern is a two-dimensional slot representing the interface between the combustor and first

Table 1. Geometric and Flow conditions

Scaling factor	9
Scaled up chord length (C)	59.4 cm
Scaled up axial chord length	29.3 cm
Pitch / chord (P/C)	0.77
Span / chord (S/C)	0.93
Re_{in}	2.1×10^5
Inlet and exit angles	0° & 72°
Inlet, exit Mach number	0.017,0.085
Inlet mainstream velocity	6.3 m/s

Table 2. Summary of Endwall Geometry

	Parameter	Experimental
Mid-Passage Gap	W - Passage gap width	0.01C
	H - Seal strip thickness	0.5W
	A - Thermocouple location	6H
	B - Passage gap depth	10H
	C - Seal strip gap	2H
	D - Seal strip width	16.8H
	E - Passage gap plenum width	28H
Upstream Slot	Upstream Slot width	0.024*C*
	Slot flow length to width	1.88
Film Cooling	FC hole diameter (cm)	0.46
	FC Hole L/D	8.3

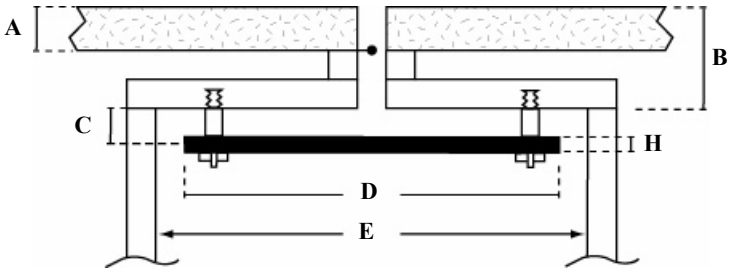

Figure 2. Cross section view (section AA, Figure 1) of the mid-passage gap plenum and accompanying seal strip (see Table 2).

stage of the turbine. This slot is located 30% of the axial chord upstream of the vane stagnation location and is designed to be forward facing with an injection angle of 45° with respect to the endwall surface. This leakage interface will be referred to as the upstream slot. Table 1 provides a description of turbine vane geometry and operating conditions and Table 2 provides a summary of parameters relevant to film-cooling and upstream slot geometries.

The focus of this paper, as explained, is the interface

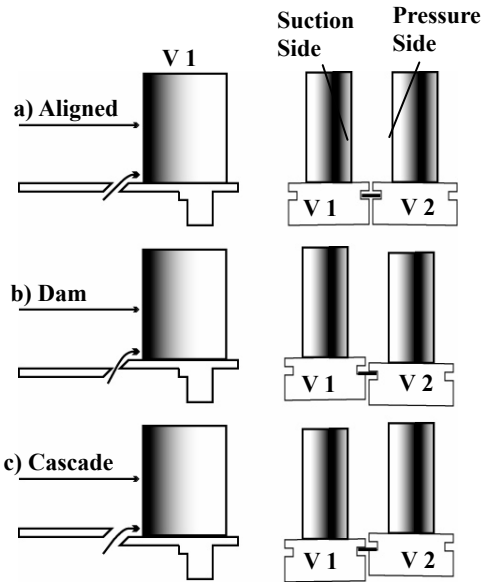

Figure 3. Side and upstream views of the three alignment modes for two adjacent vane platforms.

between adjacent vane sections, which we will refer to as the mid-passage gap. Unlike the upstream slot, the mid-passage gap has a recessed seal strip that can affect its interaction between the surrounding coolant and mainstream flows. Also, the mid-passage gap does not open into the upstream slot and has its own supply plenum. The dimensions and arrangement of the mid-passage gap plenum is shown in Table 2 and Figure 2. The vane-to-vane interface has three distinct alignment modes: aligned, forward facing step (dam), and backward facing step (cascade). The aligned mode, which is shown in Figure 3a, represents no disparity in height between adjacent vanes and the combustor.

The offset that was considered for the misaligned endwall was 1.2% of vane height or 0.65 cm for the 9X scale geometry. The dam endwall refers to a condition where the suction surface of vane 1 (V1) is raised relative to the pressure side of vane 2 (V2) which is flush with the combustor wall. This configuration is referred to as a dam because, as the secondary flows are driven from the pressure side of one vane towards the suction side of the adjacent vane, the flow faces an upward step. Figure 3b shows the dam configuration has a raised step for V1 at the upstream slot location.

The cascade endwall refers to a condition where the suction surface of V1 is lowered relative to the pressure side of the V2, which is flush with the combustor wall as shown in Figure 3c. This configuration is referred to as a cascade because the secondary flows from the pressure to the suction side experience a waterfall, or cascade, effect. For the cascade case, the upstream slot has a recessed step for the vane 1 portion of the platform.

Relative to the work that was done by Knost and Thole [12], endwall roughness was also investigated. For this simulation, the study completed by Bons et al. [17] was referenced to model realistic surface roughness on a first stage vane platform. Bons et al. lists measured values of endwall rms roughness height (R_a) as 28 μm. This rms value translates to a

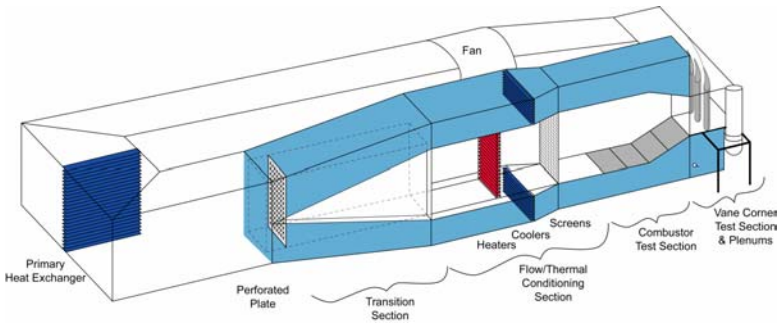

Figure 4. Illustration of the wind tunnel facility.

equivalent sand grain roughness of 227 microns for a 9X wind tunnel simulation scale (as described by Bogard et al. [18]), which is the scaling factor for the test vane. At 9X scale, this resulted in equivalent sandgrain roughness (k_s) of 1.74 mm.

To simulate a uniformly rough surface, wide-belt industrial sandpaper was used to cover the entire endwall. It has a closed-coat 36 grit surface and grade Y cloth backing. The 36 grit sandpaper corresponds to sand grain roughness of 642 microns (www.sizes.com/tools/sandpaper.htm), which is slightly above the corresponding values in the engine. A closed-coat surface has roughness elements arranged in a random array over 100% of the surface. Custom construction of the sandpaper was used to guarantee tight tolerances around each film-cooling hole. This ensured that the rough surface does not block the hole and that the interaction between the rough surface and coolant jets is uniform for the entire endwall.

EXPERIMENTAL METHODOLOGY

The experimental facility included a test section placed in a wind tunnel as shown in Figure 4. The test section consisted of a vane scaled up by a factor of nine with cooling holes and slot geometries. Adiabatic endwall temperature measurements were taken for different flowrates through film-cooling holes and through the slot representing the combustor turbine interface. For the present study, there was no flow through the mid-passage gap at the interface of the vanes. This was primarily done to study the aerodynamic effect caused by the presence of the gap and to simulate a perfectly sealed interface.

The test section was placed inside the closed-loop wind tunnel facility shown in Figure 4 and a detailed account of its construction has been previously described by Knost and Thole [12]. The difference in this test section from the one used by Knost and Thole is the presence of a rough endwall surface and the presence of a mid-passage gap between the endwalls of the adjacent vanes. The flow in the wind tunnel is driven by a 50 hp axial vane fan, which is controlled by variable frequency inverter. Downstream of the fan, the flow encounters a 90° turn and passes through a primary finned-tube heat exchanger used to cool the bulk flow. After the heat exchanger, the flow encounters a three-way flow split. Note that only the bottom channel was used for this study. This split was done to create a primary core flow and a cooled secondary flow. The primary

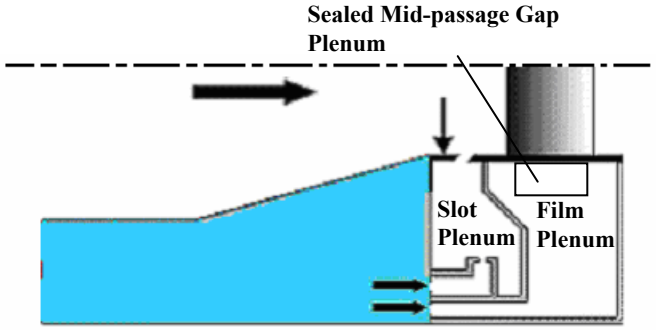

Figure 5. Separate plenums for film-cooling and upstream slot provided independent control of the flow through each of them.

core flow was made to pass through a heater bank consisting of three heaters where the air temperature was increased to 55°C. The secondary flow, in the outer channel, was made to pass through a secondary heat exchanger where the flow temperature was lowered to about 15°C. The secondary flow path represented the coolant flow through the film-cooling holes and the slots.

The test section consisted of two full passages with one center vane and two half vanes. It is important to note that film-cooling effectiveness studies were done only in the passage where the mid-passage gap was simulated. The test section consisted of separate plenums for independent control of flow through the film-cooling holes and the upstream slot as shown in Figure 5. A temperature difference of about 40°C was maintained at all times between the mainstream and coolant flows under steady state conditions.

Typical times to achieve steady state conditions were 3 hours. The freestream turbulence effects were not taken into consideration as these studies were more focused on industrial gas turbines rather than on aero engines. Freestream turbulence levels are generally higher for aero engines when compared to industrial gas turbines. The inlet turbulence effects and length scales were however measured to be 1.3% and 4 cm respectively.

The endwall of the vane, which was the main focus of study, was constructed of foam because of its low thermal conductivity (0.033 W/m.K). The endwall foam was 1.9 cm thick and was mounted on a 1.2 cm thick Lexan plate. The cooling hole pattern on the endwall was cut with a five-axis water jet to ensure precision and integrity. The upstream slot was constructed with hard wood as it had a low conductivity and was stiffer.

Coolant Flow Settings

For every test condition the dimensionless pressure coefficient distribution was verified to ensure periodic flow through the passages. As stated earlier two separate plenums were used to control the flowrate through the film-cooling holes and through the upstream slot. Friedrichs et al. [5] suggested that a global blowing ratio based on the inlet flow conditions could be characterized by the blowing ratio of a loss-free hole injecting into inlet conditions calculated from:

Table 3. Summary of Coolant Settings

%mass flow	C_D	M_{ideal}	M_{actual}
0.35 Film Cooling	0.85	1.24	1.06
0.50 Film-Cooling	0.8	1.88	1.51
0.75 Film-Cooling	0.71	3.2	2.26
0.75 Upstream Slot	0.6	0.48	0.29
0.95 Upstream Slot	0.6	0.69	0.414
1.10 Upstream Slot	0.6	0.72	0.43

$$M_{ideal} = \sqrt{\frac{\rho_c}{\rho_{in}} \frac{P_{o,c} - p_{s,in}}{P_{o,in} - p_{s,in}}} \quad . \qquad (1)$$

A modification of this approach was done in this study and a global discharge coefficient, C_D, was derived so that a cumulative flowrate through the film-cooling holes could be defined. These C_D values were obtained from CFD studies done on a similar geometry and have been reported earlier by Knost and Thole [11]. Measurements of the inlet velocity, average inlet static pressure, and coolant total pressures were obtained which then allowed the fraction of coolant flow relative to the inlet core flow to be calculated from:

$$\frac{\dot{m}_c}{\dot{m}_{core}} = M_{ideal} . C_D . \frac{A_{hole}}{A_{in}} . \#\,holes \qquad (2)$$

The upstream slot flow was assumed to have a discharge coefficient of 0.6 which is the assumed value for a flow through a sharp-edged orifice and the flowrate was calculated accordingly. Table 3 gives a description of the actual and ideal global blowing ratios used for the different film-cooling and upstream slot mass flowrate settings.

Instrumentation and Temperature Measurements

An Inframetrics P20 infrared camera was used to capture the spatially-resolved adiabatic wall temperatures on the endwall. Measurements were taken at seven different viewing locations to ensure that the entire endwall surface was mapped. The camera was placed perpendicular to the endwall surface at a distance of 55 cm. Each picture covers an area 24 cm by 18cm, with the area being divided into 320 by 240 pixel locations. The spatial integration of the camera was 0.715 mm (0.16 hole diameters). Thermocouples were also placed on the endwall surface at different locations to directly measure the temperature to post calibrate the infrared images. For the post calibration the emissivity and background temperature were adjusted until the temperatures from the infrared camera images were within 1ºC of the corresponding thermocouple data. Typical emissivity values and background temperatures were 0.92 and 45ºC (note that the freestream temperature was 55ºC). Seven images were taken at each of the viewing locations to

obtain an averaged picture using an in-house Matlab program. The same program was also used to assemble the averaged pictures at all locations to give a complete temperature distribution along the passage endwall.

Freestream temperatures were measured at multiple locations along the pitch and the average was determined by using a thermocouple rake consisting of three thermocouples along the span. It was found that the variations along the pitch were less than 0.2ºC and that along the span were less than 1.5ºC. Three thermocouples were attached in the upstream slot location at the combustor exit, and two thermocouples were attached in the film-cooling plenum. Eleven thermocouples were placed in the mid-passage gap to measure the temperature profile along the gap. The thermocouples in the mid-passage gap were placed six strip seal thicknesses beneath the surface, which was roughly one-third of the slot flow length beneath the surface (Table 2). Voltage outputs from the thermocouples were acquired by a 32 channel data acquisition module that was used with a 12-bit digitizing card. The temperature data was compiled after the system reached steady state.

An uncertainty analysis was performed on the measurements of adiabatic effectiveness using the partial derivative method described at length by Moffat [19]. The precision uncertainty was determined by taking the standard deviation of six measurement sets of IR camera images with each set consisting of five images. The precision uncertainty of the measurements was ±0.014°C. The bias uncertainty was ±1.0°C based on the calibration of the image. The bias uncertainty of the thermocouples was ±0.5°C. The total uncertainty was then calculated as ±1.0°C for the images and ±0.51°C for the thermocouples. Uncertainty in effectiveness, η, was found based on the partial derivative of η with respect to each temperature in the definition and the total uncertainty in the measurements. Uncertainties of $\partial\eta = \pm 0.082$ at $\eta = 0.2$ and $\partial\eta = \pm 0.029$ at $\eta = 0.9$ were calculated. A one-dimensional conduction analysis was performed at the entry and exit of the passage to calculate the conduction error. The resulting η correction was found to be 0.07 at the entrance and 0.02 at the exit region at a measured η value of 0.5.

DISCUSSION OF RESULTS

As stated previously, all tests and data acquisition were completed for no flow through the mid-passage gap. First, the effect of the presence of the mid-passage gap and roughness will be discussed for an aligned endwall. The results from this test will be compared with an existing case having no mid-passage gap. Second, a comparison of results obtained for aligned and misaligned mid-passage gap will be discussed.

Film-Cooling Effectiveness with a Rough Endwall and a Mid-Passage Gap

The nominal film-cooling cases with and without a mid-passage slot for 0.75% upstream slot flow and 0.5% film-cooling flow are shown in Figure 6a-b. Note that the

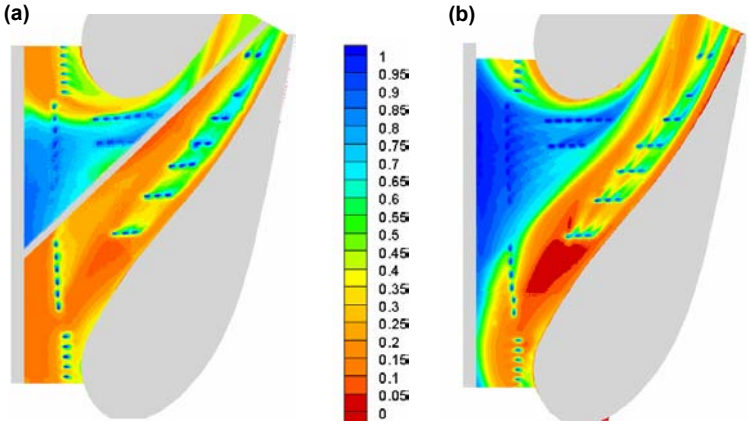

Figure 6a-b. Contours of adiabatic effectiveness for film-cooling cases (a) rough endwall with mid-passage slot (b) smooth endwall with no mid-passage slot.

percentages refer to the coolant flow relative to the hot gas path flow. There are two noticeable effects that can be determined by comparing these two cases that include the effect of the mid-passage gap and the effect of roughness.

It can be seen from Figure 6a that there is no coolant flow from the upstream slot crossing over the mid-passage gap location. This condition becomes apparent when comparing the contours of Figure 6a with those of Figure 6b where, in the absence of the gap, the coolant from the upstream slot convects towards the suction side of the vane sweeping over a large area of the endwall. In the presence of the mid-passage gap, Figure 6a shows no coolant exiting the upstream slot on the pressure side of the mid-passage gap. The reason for this lack of coolant is that the coolant from the upstream slot is ingested until the end of the vane passage where it then exits the gap. This effect will be discussed further in a later section of the paper. As a result of this degradation of the coolant on the pressure side of the mid-passage gap, the hot streak through the center of the passage appears to be wider with the presence of a mid-passage gap relative to the no gap case. In determining the effect of roughness on the endwall film-cooling, comparisons can also be made between Figures 6a and 6b.

Observing the coolant exiting from the leading edge holes upstream of the stagnation location on the suction side, one can see that the coolant is dispersed more rapidly for the case with the rough endwall relative to the smooth endwall. Along the pressure side, the jets merge more evenly in the case of the rough endwall relative to the smooth endwall where in the case of the smooth endwall there are distinct jets.

To quantify the effects of roughness, a section of the endwall near the pressure side of the vane, as shown in Figure 7, was further analyzed. Figures 7a and 7b show the effect of roughness on the laterally averaged effectiveness for 0.5% and 0.75% film-cooling flows, respectively. Also indicated in Figure 7 are the row-averaged local blowing ratios for each row of holes along the pressure side. Note that CFD results were used to quantify the local coolant flows from each cooling

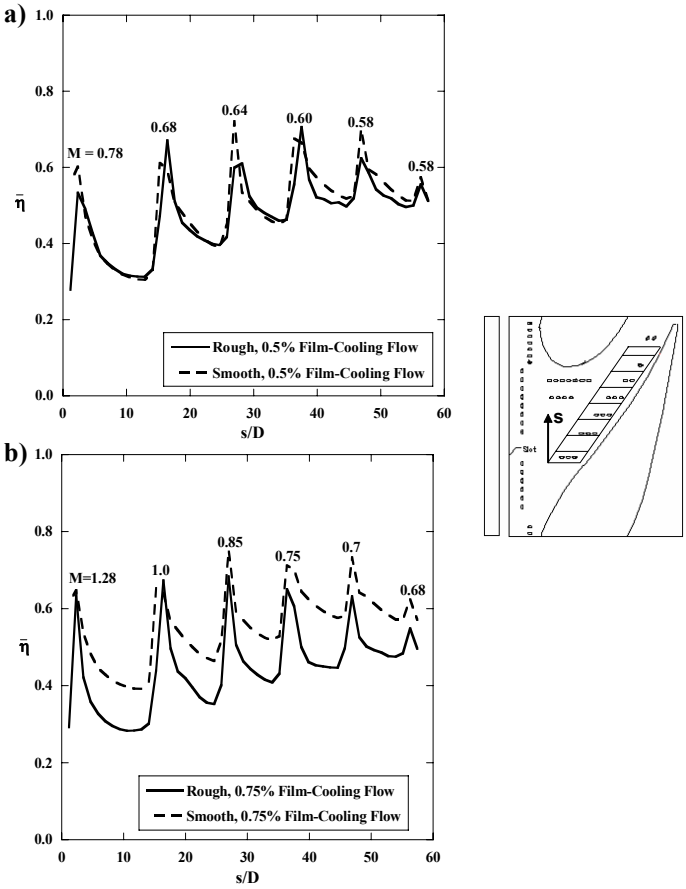

Figure 7a-b. Plots of laterally averaged adiabatic effectiveness on the film-cooling holes on the pressure side: (a) for 0.75% upstream slot flow and 0.5% film-cooling and (b) 0.75% upstream slot flow and 0.75% film-cooling.

hole and the local static pressure was used to calculate the local freestream velocity that was used in the blowing ratio definition. For the 0.5% case, where the local blowing ratios ranged from 0.58 and 0.78, the laterally averaged effectiveness values indicate that there is essentially no effect of roughness of the film-cooling performance. In looking at the contours in Figure 6a and 6b, however, there are some local differences indicated particularly with the jet merging.

For the higher coolant flow condition in Figure 7b, where the local blowing ratio ranges from 0.68 to 1.28, there is a dramatic decrease in the average effectiveness along the pressure side with roughness. The decrease in the laterally averaged effectiveness due to roughness is on the order of 30% mid-way between film-cooling rows. One plausible reason that there is a larger decrease at the higher blowing ratio relative to the lower blowing ratio is because for a rough wall the boundary layer is thicker thereby allowing the jets to separate from the endwall. As the front jet separates from the wall, this effect is compounded as one progresses downstream along the pressure side. This reduction in film-cooling effectiveness may also be attributed to increased interaction with hot mainstream.

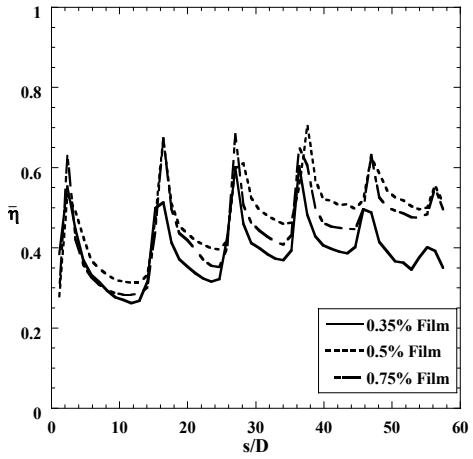

Figure 8. Laterally averaged adiabatic effectiveness for 0.35%, 0. 5% and 0.75% film-cooling flows for a rough endwall.

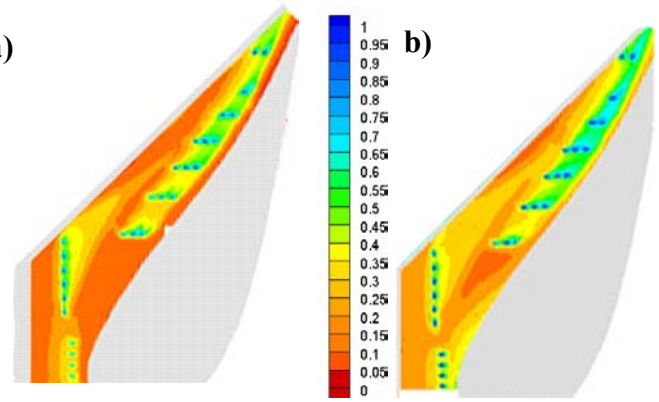

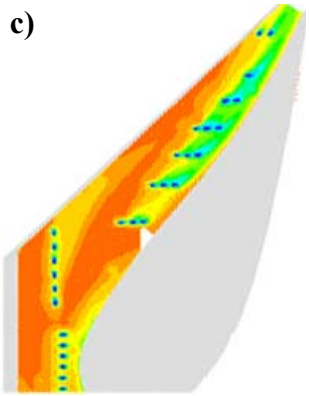

Figure 9a-c. Contours of adiabatic effectiveness with a rough endwall with 0.75% slot flow for (a) 0.35% film-cooling (b) 0.5% film-cooling (c) 0.75% film-cooling.

The rough surface greatly increases boundary layer thickness and turbulence levels, causing enhanced mixing between the

coolant and mainstream and thereby lowering area averaged values of adiabatic effectiveness.

In comparing Figures 7a and 7b, it is seen that there is a benefit in cooling when increasing the coolant flow from 0.5% to 0.75% for the smooth wall case. In contrast, when increasing the coolant flow for the rough wall case, the average adiabatic effectiveness levels actually decrease with an increase in blowing ratio. As such, Figure 8 compares the laterally averaged effectiveness values for the rough endwall case along the pressure side holes for three different coolant flowrates: 0.35%, 0.5% and 0.75%. The corresponding contours for these lateral averages just along the pressure side are shown in Figures 9a-9c. As is typically expected, by increasing the film-cooling flow from 0.35% to 0.5%, one sees that there is an increased gas performance in the film-cooling effectiveness levels. In comparing the contours shown in Figures 9a and 9b, it is clear that the first row of holes in the averaging area defined in Figure 7 appears nearly the same between the two cases, but that cooling appears to be much better at the second row for the higher blowing ratio case.

By increasing the coolant flow to 0.75%, the laterally averaged effectiveness significantly decreases relative to the 0.5% coolant flow case but is better than the 0.35% coolant flow case, as shown in Figure 8. The contours in Figure 9c indicate better penetration towards the pressure side of the endwall for the 0.75% coolant flow case, but that the overall levels of effectiveness downstream of the film-cooling holes are significantly lower than for the 0.5% coolant flow case. These contours indicate that as the jets penetrate closer to the pressure side surface, they are also lifted off the surface. Knost and Thole [11] observed a similar trend for the smooth wall case in that the pressure side film-cooling jets appeared to be lifted off the surface for the 0.75% coolant flow case, but as seen from Figure 7b this effect is worsened with roughness.

Outside of the averaging area, at the most upstream row of film-cooling holes, the contours in Figure 9a-9c indicate little change in effectiveness levels as a function of increased coolant levels. There was only slightly better performance for the 0.5% coolant flow condition relative to the 0.35% and 0.75% coolant flows. Just upstream of the stagnation location, the contours in Figures 9a-9c indicate that for the 0.5% and 0.75% coolant flow conditions, the leading edge film-cooling jets are impacting the vane and then being washed back down onto the surface indicating some coolant at the vane-endwall junction.

Effect of a Misaligned Mid-Passage Gap

One of the primary questions raised for this work was how to best design an endwall simulating the surface roughness and turbine vane misalignment. As was discussed previously, there is a possibility for an aligned endwall configuration, a cascade endwall configuration, and a dam endwall configuration. The misalignment value was set to 1.2% of the vane span. For these comparisons, both the film-cooling and upstream slot flows remained constant at 0.5% of the core flow. Figures 10a-10c corresponds to aligned, dam, and cascade endwall

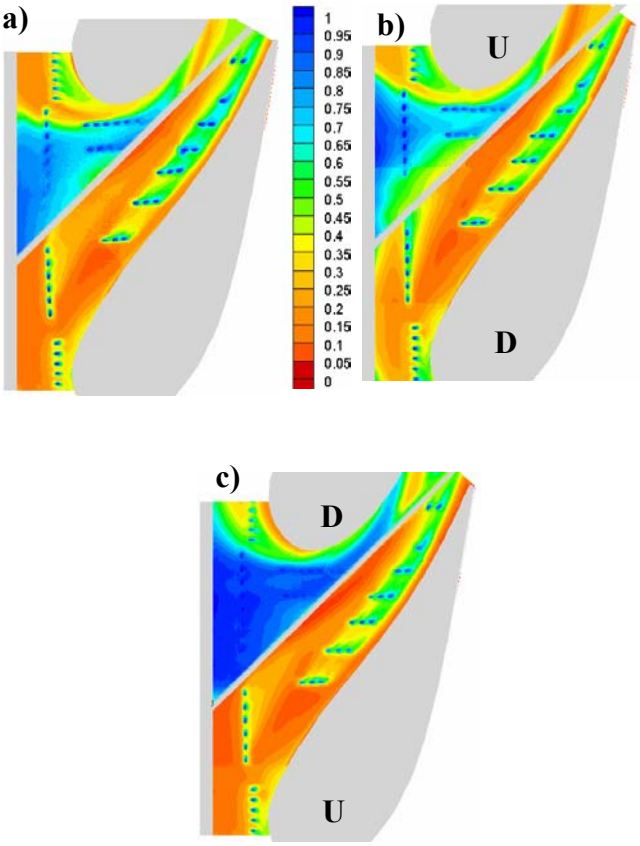

Figure 10a-c. Contours of adiabatic effectiveness on a rough endwall for the baseline film and slot cooling cases: (a) aligned) (b) dam and (c) cascade endwall (note that U refers to raised side and D refers to lowered side).

configurations respectively. Indicated on the vanes on these figures is the portion of the endwall that is raised (U) and lowered (D). For explanatory purposes, the section of endwall closest to the top vane picture is referred to as the suction side section and the section of the endwall closest to the bottom vane will be referred to as the pressure side section.

In comparing the aligned case to the dam case, it can be seen that in the case of the dam the overall platform cooling is much worse than in the case of the aligned endwall. It appears that because of the front slot misalignment, the leakage coolant from the upstream slot is directed into the hot gas path rather than along the endwall. It is also interesting to look at the end of the mid-passage gap. Figure 10a for the aligned endwall indicates that at the mid-passage gap exit, coolant exits the slot. This coolant was the upstream slot coolant and film-coolant that was ingested into the slot and then exited at the lowest external static pressure location. In the case of the dam endwall, Figure 10b indicates that there is no coolant exiting the end of the mid- passage slot. It is also quite interesting to see the diminished effectiveness levels in the vicinity of the mid-passage slot at about 20% of the slot length measured from

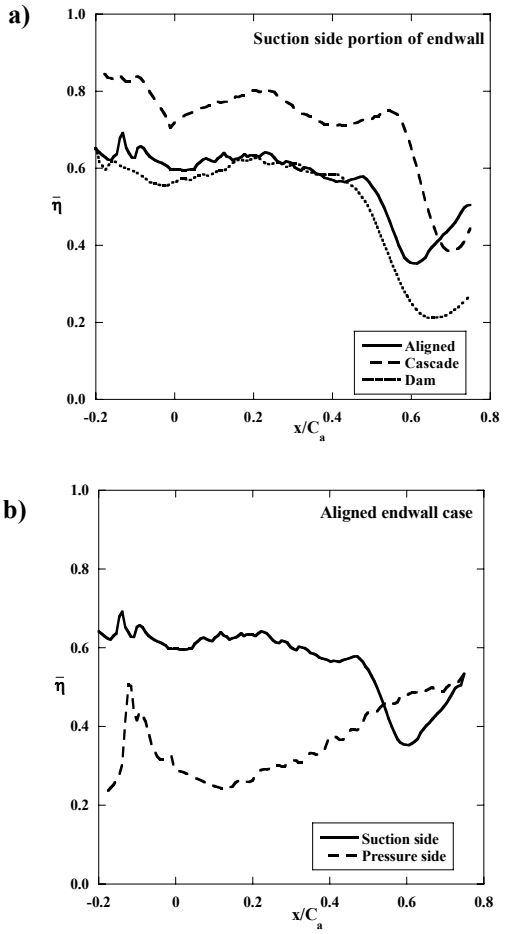

Figure 11. Pitch-wise averaged adiabatic effectiveness for the baseline film and slot cooling cases: a) along the suction side for the three endwall settings b) comparison between effectiveness on the suction and pressure side.

the upstream slot shown in Figure 10b. This warmer region was also shown for aligned endwall in Figure 10a, but it is not as dramatic. At this location, there is no upstream slot flow, present, which was worsened for the dam configuration, nor is there any film- cooling flow present.

When the endwall surface is set to cascade configuration, coolant from the upstream slot can flow in an unobstructed manner onto the endwall. The effectiveness contours in Figure 10c indicate a much improved performance for the cascade case relative to both the aligned and the dam configurations. The lowered endwall in the case of the cascade acts like a trough in which the upstream slot flow does not mix out as quickly with the mainstream hot gas. As a result, higher effectiveness values occur on the suction side portion of the endwall. For the cascade configuration, the pressure side contours are very similar to the aligned endwall configuration, because there is no blockage for the secondary flows, as compared with the dam case. At 20% slot length downstream from the upstream slot the warm region previously discussed is diminished for the cascade condition relative to both the dam

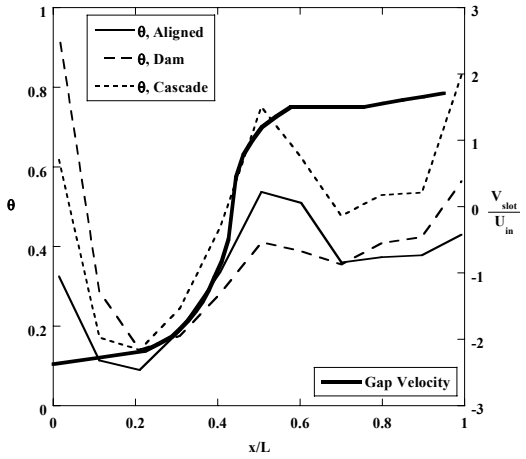

Figure 12. Non-dimensionalized gap temperature profiles for the three endwall alignment modes and the velocity profile for an aligned gap.

and aligned cases.

Figure 11a compares the pitchwise-averaged effectiveness along the suction side of the endwall for the three endwall configurations and Figure 11b compares the effectiveness distribution along the suction and pressure sides for the aligned case. Figure 11a clearly substantiates the previous results that the cascade configuration results in better cooling along the suction side and Figure 11b strengthens the conclusion that there is better cooling on the suction side than on the pressure side for any kind of endwall configuration. It was also found that the pitch-wise averaged effectiveness on the pressure side for the three endwall settings remained the same. The area-averaged effectiveness was higher for the cascade configuration when compared to the aligned or dam. The area-averaged effectiveness levels, which include both the pressure and suction side portions of the endwall, were 0.49 for cascade, 0.45 for the aligned and 0.42 for the dam respectively.

As was previously discussed, the air temperature inside the gap was measured as indicated in Figure 2. Recall that for the study reported in this paper there was no flow exiting the mid-passage gap such that the temperatures measured were those of any flow that might ingest into the mid-passage slot. The measured non-dimensional gap temperatures for the aligned and misaligned cases are shown in Figure 12. The non-dimensionalization was based on the coolant temperature and hot gas freestream temperatures. Also shown in Figure 12 are the inviscid gap velocities that were calculated based on the local static pressure at the gap exit. Note that this inviscid analysis assumed a constant total pressure difference between the mainstream and the gap plenum. An iterative procedure was used to calculate the pressure difference which resulted in zero net mass flow from the slot (ingested flow balanced with exiting flow).

Figure 12 shows that for the aligned and dam cases, a large amount of coolant is ingested into the leading edge of the mid-passage gap region relative to the cascade case. In the location

0<x/L<0.2 there is coolant ingestion from the upstream slot resulting in higher θ, with the amount of coolant being ingested decreasing with an increase in x/L. There is also increased ingestion of the mainstream flow causing a rapid rise in the gap air temperature and hence a decrease in θ. The non-dimensional temperatures in the gap decrease dramatically as hot mainstream flow is ingested near x/L = 0.2. For the mid-passage gap location between 0.3 < x/L < 0.5, all of the endwall cases show a decrease in the air temperature (increase in θ) along the mid-passage gap, which results from a fresh influx of coolant from the two rows of film-cooling holes directly upstream of this region (see Figure 10a-c). The dam case benefits less because of the step, in conjunction with the cross passage secondary flows that forces more hot flow into the gap. Figure 12 also shows that the temperatures inside the gap associated with the cascade endwall setting are cooler than that for the dam endwall setting, which is because of the cooler fluid from the upstream slot. Up to x/L = 0.5, the inviscid velocity is indicated to be into the slot (static endwall pressure is higher than the plenum pressure), which is consistent with the fact that flow is ingesting into the slot.

Beyond x/L = 0.5, Figure 12 shows that flow exits the mid-passage gap. Between 0.5 < x/L < 0.7, there is an increase in the temperature within the mid-passage gap, which is followed by a decrease beyond x/L = 0.9. The slight increase at the exit results from any coolant that was channeled through the mid-passage gap from the upstream slot.

Effect of Slot Flow with a Cascade Endwall

Because the best configuration appeared to be the cascade endwall, more studies were completed with this configuration whereby flow from the upstream slot was varied. As previously discussed, the coolant flow from upstream slot has little effect on the pressure side of the mid-passage slot. Figure 13 compares adiabatic effectiveness contours for different slot flowrates (or different momentum flux ratios) with cascade endwall setting. The momentum flux ratios were calculated for all the flowrates through the slot using the relation,

$$I = \frac{\rho_s u_s^2}{\rho_\infty U_\infty^2} = \frac{\rho_s (\dot{m}/\rho_s A_s)^2}{\rho_\infty U_\infty^2} \qquad (3)$$

It can be seen in Figure 13a, that for 0.75% slot flow there is little cooling around the leading edge holes on the pressure side. With an increase in the slot flowrate, however, the adiabatic effectiveness near the upstream slot region increases, indicating some coolant exiting from the upstream slot onto the pressure side of the mid-passage gap as seen in Figure 13b and Figure 13c. It is also interesting that as the upstream slot flow is increased, the warmer region is no longer present that was shown at the 0.75% coolant flow condition about one-third of the way downstream of the mid-passage slot. It is also interesting to note that the film-cooling holes on the pressure side of the mid-passage gap showed better cooling as the slot flow was increased to 0.95% relative to 0.75%.

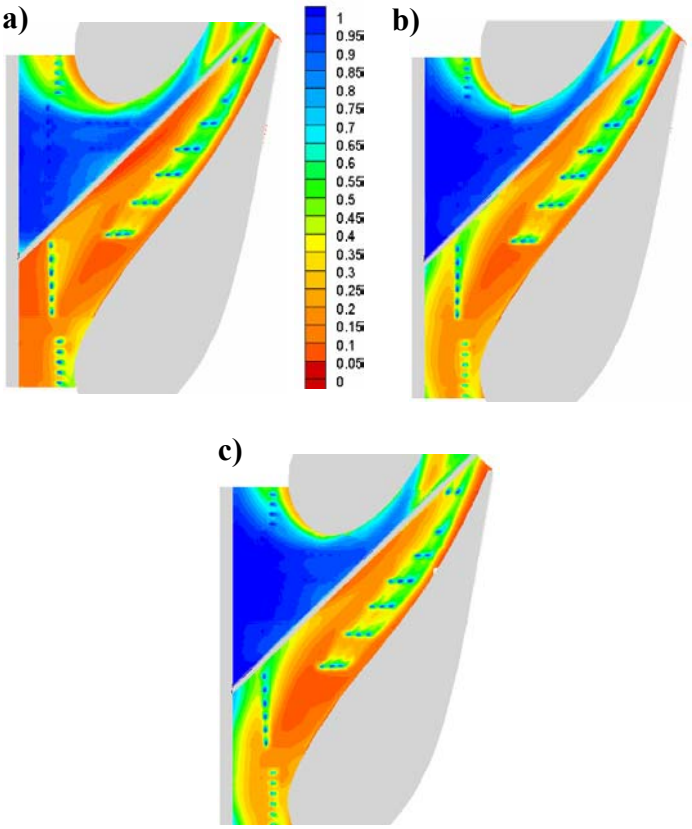

Figure 13a-c. Contours of adiabatic effectiveness on a rough endwall with cascade setting for different upstream slot flowrate with 0.5% film-cooling: (a) 0.75% (I = 0.08) slot flow, (b) 0.95% (I = 0.12) slot flow, (c) 1.1% (I = 0.16) slot flow.

CONCLUSIONS

Measurements of endwall and mid-passage gap adiabatic effectiveness were presented for an endwall surface with realistic features, namely a combustor to turbine interface gap, endwall film-cooling, a vane to vane mid-passage gap, a platform misalignment, and surface roughness. When compared to a smooth surface, it was observed that the effect of roughness could vary. For the higher blowing ratio, there was a definite decrease in adiabatic effectiveness due to roughness but for the lower blowing ratio, there was essentially no difference in cooling. This difference was related to the boundary layer thickness whereby a thicker boundary layer had a significant impact on the jet separation from the endwall in the case of a high blowing ratio.

The mid-passage gap had a significant impact on the progression of the upstream coolant whereby the gap limited the area of coverage for the upstream slot coolant flow. The cooling from the upstream slot had a beneficial effect only along the suction side surface of the vane. Measurements along with an inviscid analysis indicated that fluid from the platform was ingested into the mid-passage gap. Near the start of the gap, most of the flow ingested was coolant, which

rapidly decayed because of the hot gas ingested.

Platform misalignment proved to also have a substantial effect on endwall adiabatic effectiveness levels. Clearly, from a heat transfer standpoint, a cascade configuration would be the most desirable endwall alignment mode. The cascade setting showed considerably better adiabatic effectiveness levels relative to an aligned or dam endwall configuration nearly removing the need for cooling holes on the suction side of the endwall. From a turbine design standpoint, the cascade setting is ideal relative to a dam configuration as the cascade acts like a trench where the coolant flow can reside.

This study has shown the drastic effects that realistic turbine features can have on first stage nozzle platform cooling. Upstream slot flow and a cascade misalignment provide for better cooling on the endwall. Quite the opposite is the case for a misaligned dam, mid-passage gap, and, in some cases, endwall surface roughness. These competing effects, when properly understood, can be used to better design endwall cooling arrangements.

ACKNOWLEDGMENTS

This publication was prepared with the support of the US Department of Energy, Office of Fossil Fuel, and National Energy Technology Laboratory. However, any opinions, findings, conclusions, or recommendations expressed herein are solely those of the authors and do not necessarily reflect the views of the DOE. The authors would also like to thank Mike Blair (Pratt & Whitney), Ron Bunker (General Electric), and John Weaver (Rolls-Royce) for their input on the modeling of realistic turbine features.

REFERENCES

[1] Blair, M.F., 1974, "An experimental Study of Heat Transfer and Film-cooling on Large-Scale Turbine Endwall," *ASME J of Heat Transfer*, vol. 96, pp. 524-529.

[2] Burd, S.W., Satterness, C.J., and Simon, T.W., 2000, "Effects of Slot Bleed Injection Over a Contoured Endwall On Nozzle Guide Vane Cooling Performance: Part II - Thermal Measurements," 2000-GT-200.

[3] Colban, W. F., Thole, K. A., and Zess, G., 2002, "Combustor-Turbine Interface Studies: Part 1: Endwall Measurements," *J of Turbomachinery*, vol. 125, pp.193-202.

[4] Colban, W. F., Lethander, A. T., Thole, K. A., and Zess, G., 2002, "Combustor-Turbine Interface Studies: Part 2: Flow and Thermal Field Measurements," *J of Turbomachinery,* vol. 125, pp.203-209.

[5] Friedrichs, S., Hodson, H. P. and Dawes, W. N., 1996, "Distribution of Film-Cooling Effectiveness on a Turbine Endwall Measured Using the Ammonia and Diazo Technique," *J of Turbomachinery*, vol. 118, pp. 613-621.

[6] Friedrichs, S., Hodson, H. P. and Dawes, W. N., 1997, "Aerodynamic Aspects of Endwall Film-Cooling," *J of Turbomachinery*, vol. 119, pp. 786-793.

[7] Friedrichs, S., Hodson, H. P. and Dawes, W. N., 1999, "The Design of an Improved Endwall Film-Cooling Configuration," *J of Turbomachinery*, vol. 121, pp. 772-780.

[8] Zhang, L.J., and Jaiswal, R.S., 2001, "Turbine Nozzle Endwall Film-cooling Study Using Pressure Sensitive Paint," *J of Turbomachinery*, **123**, pp. 730-738.

[9] Kost, F. and Nicklas, M., 2001, "Film-Cooled Turbine Endwall in a Transonic Flow Field: Part I – Aerodynamic Measurements," ASME Paper Number 2001-GT-0145.

[10] Nicklas, M., 2001, "Film-Cooled Turbine Endwall in a Transonic Flow Field: Part II – Heat Transfer and Film-Cooling Effectiveness," *J of Turbomachinery*, **123**, pp. 720-729.

[11] Knost, D.G., and Thole, K.A., "Computational Predictions of Endwall Film-Cooling for a First Stage Vane," GT2003-38252.

[12] Knost, D. G., and Thole, K. A., "Adiabatic Effectiveness Measurements of Endwall Film-Cooling for a First Stage Vane," *J of Turbomachinery*, GT2004-52236.

[13] Yu, Y., and Chyu, M.K., 1998, "Influence of Gap Leakage Downstream of the Injection Holes on Film-cooling Performance," *J of Turbomachinery*, **120**, pp. 541-548.

[14] Aunapu, N.V., Volino, R.J., Flack, K.A., and Stoddard, R.M., 2000, "Secondary Flow Measurements in a Turbine Passage with Endwall Flow Modification," *J of Turbomachinery*, **122**, pp. 651-658.

[15] Ranson, W., Thole, K. A., and Cunha, F., "Adiabatic Effectiveness Measurements and Predictions of Leakage Flows Along a Blade Endwall" IMECE2004-62021.

[16] Yamao, H., Aoki, K., Takeishi, K., and Takeda, K., 1987, "An Experimental Study for endwall Cooling Design of Turbine Vanes," IGTC-1987, Tokyo, Japan.

[17] Bons, J.P., Taylor, R.P., McClain, S.T., and Rivir, R.B., 2001, "The Many Faces of Turbine Surface Roughness," 2001-GT-0163.

[18] Bogard, D. G., Schmidt, D. L., Tabbita, M., 1998, "Characterization and Laboratory Simulation of Turbine Airfoil Surface Roughness and Associated Heat Transfer," *J of Turbomachinery*, vol. 120, pp. 337-342.

[19] Moffat, R. J., "Describing the Uncertainties in Experimental Results," *Experimental Thermal and Fluid Science*, Vol.1, pp. 3-17.